University of Groningen

Experimental study of the structure of laminar axisymmetric H2/air diffusion flames

Toro, Vishal Vijay

IMPORTANT NOTE: You are advised to consult the publisher's version (publisher's PDF) if you wish to cite from it. Please check the document version below.

Document Version
Publisher's PDF, also known as Version of record

Publication date:
2006

Link to publication in University of Groningen/UMCG research database

Citation for published version (APA):
Toro, V. V. (2006). *Experimental study of the structure of laminar axisymmetric H2/air diffusion flames*. s.n.

Copyright
Other than for strictly personal use, it is not permitted to download or to forward/distribute the text or part of it without the consent of the author(s) and/or copyright holder(s), unless the work is under an open content license (like Creative Commons).

The publication may also be distributed here under the terms of Article 25fa of the Dutch Copyright Act, indicated by the "Taverne" license. More information can be found on the University of Groningen website: https://www.rug.nl/library/open-access/self-archiving-pure/taverne-amendment.

Take-down policy
If you believe that this document breaches copyright please contact us providing details, and we will remove access to the work immediately and investigate your claim.

Downloaded from the University of Groningen/UMCG research database (Pure): http://www.rug.nl/research/portal. For technical reasons the number of authors shown on this cover page is limited to 10 maximum.

Download date: 05-05-2023

2

Experimental Techniques, Procedures and Burner Setup

2.1 General introduction

In this thesis, we study the flame structure of laminar coflow H_2/air diffusion flames by the experimental determination of the distribution of major species, reactive radicals and temperature. As indicated in the previous chapter, we use non-intrusive laser diagnostics for this purpose. Spontaneous Raman scattering is used to measure the major species (H_2, O_2, N_2 and H_2O), while the temperature is measured by both Raman scattering and CARS. Hydroxyl radicals in the flames under investigation are measured using LIF. This chapter is devoted towards describing the introductory background of these methods, the optical setups used and the experimental procedures implemented in rest of the thesis. A description of the burner schematic and the flow schemes for the gases is also provided. The quantitative aspects of these optical methods will be discussed in Ch. 3.

2.2 Spontaneous Raman scattering

2.2.1 Introduction

When radiation of frequency ν_0 passes through a gas medium, a small amount of the radiation is scattered. The scattered radiation is mainly at the same frequency as the incident radiation (Rayleigh scattering), but also contains other frequencies in pairs at $\nu_S = \nu_0 - \nu_m$ (Stokes) and $\nu_{aS} = \nu_0 + \nu_m$ (anti-Stokes) Raman scattering, respectively. These shifts in frequencies ν_m are associated with the transitions between rotational and vibrational levels. In Stokes Raman scattering, some of the energy from the laser beam is transferred to the molecule, causing a transition from the initial level (E_2) to a higher state (E_3) (Fig. 2.1). In anti-Stokes Raman scattering, the molecule ends in a lower energy state (E_1), and with the frequency shift to a higher value. In Rayleigh scattering, there is no net change in the state of the molecule.

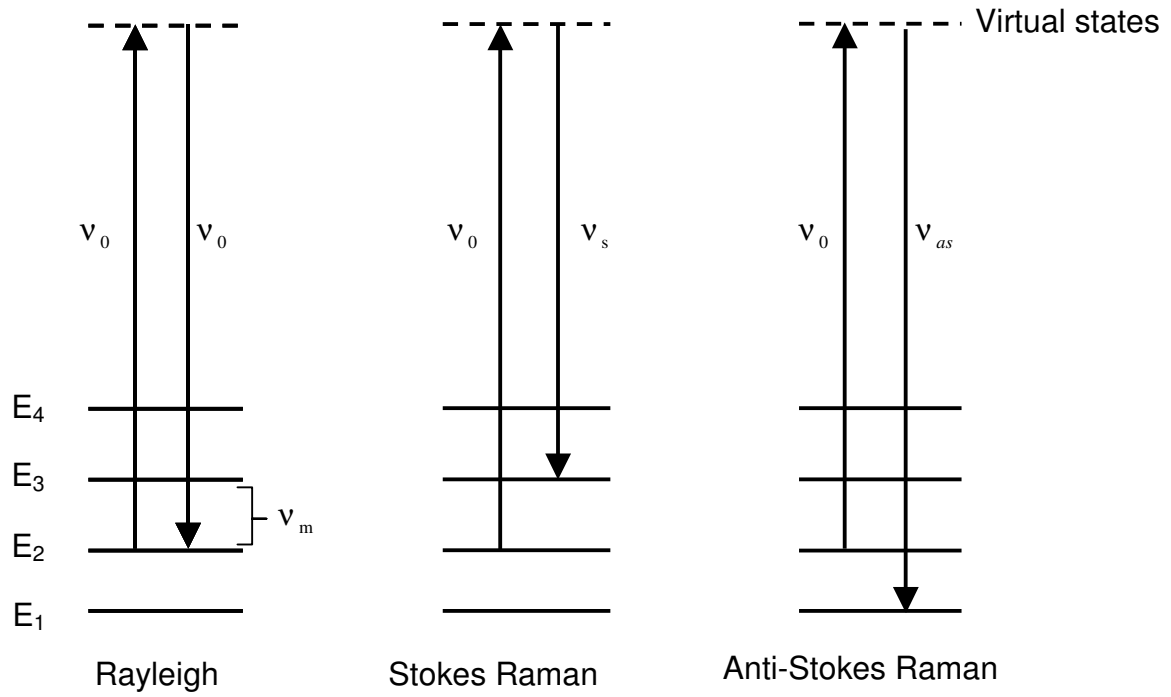

Figure 2.1 Rayleigh, Stokes and anti-Stokes Raman scattering phenomena

The intensities of Rayleigh and Raman scattering can formally be written as [1-3]

$$I = P_l N_j \left(\frac{d\sigma}{d\Omega}\right)_j \Delta\Omega \, l\varepsilon, \tag{2.1}$$

where $\left(\frac{d\sigma}{d\Omega}\right)_j$ is the Raman (or Rayleigh) cross-section of species j at certain temperature, $\Delta\Omega$ is the collecting solid angle, P_l is the incident laser power, N_j is the number density of molecules of j, l is the sampling extent, and ε is the quantum efficiency of the detecting system. In general, the Raman and Rayleigh cross-sections depend on the excitation frequency, molecular structure and direction of observation.

Spontaneous Raman scattering is now a fully established measuring technique in the experimental studies in combustion research. There is a large amount of literature providing details on experimental approaches and capabilities of this method. As an example, the interested reader is referred to review texts, such as [4] and references therein. Many researchers used this technique in different configurations, with different excitation wavelengths and with different detection schemes. For instance, Raman scattering measurements with simultaneous detection of different species were conducted at single-point in flames [5], along the laser line [6] and two-dimensional species distribution measurements [7]. Another aspect of exploiting the advantages

provided by this technique is to use different laser wavelengths. Although Raman measurements using 532 nm excitation are more common, there are also many studies using other wavelengths. In particular, the availability of narrow bandwidth ultraviolet excimer lasers led to developments in Raman studies (*e.g.* [8,9]). As the Raman cross-section scales with the frequency to the fourth power (see Ch. 3), the Raman signals obtained using ultraviolet lasers are greatly enhanced over the visible excitation, however optical alignment can be a problem. The Raman signal enhancement using ultraviolet wavelength is one option; another is the use of high repetition rate lasers to maximize Raman signals.

2.2.2 Experimental approach

The optical setup used for the Raman measurements is shown in Fig. 2.2. The second harmonic of a pulsed Nd:YAG laser (Quanta-Ray GCR-150-25, SpectrsPhysics) at 50 mJ pulse energy with 25 Hz repetition rate was focused by a quartz lens having focal length of 800 mm into the test location. The pulse energy was

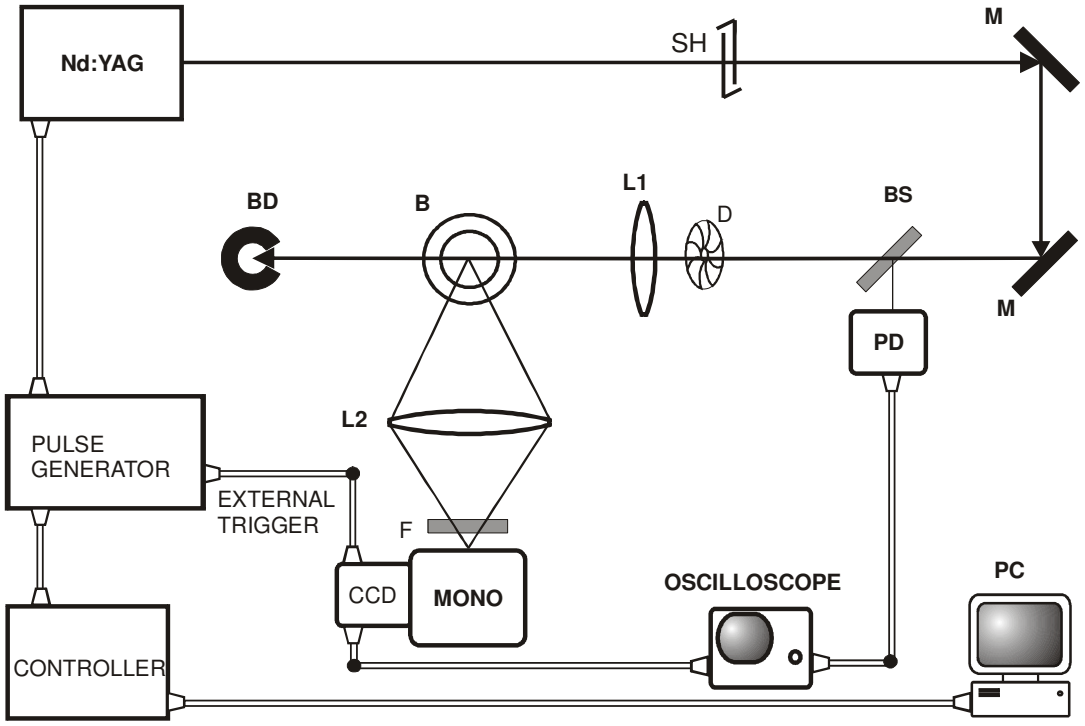

Figure 2.2 Optical setup for the Raman measurements, where SH: shutter, M: mirror, D: diaphragm, L1: focusing lens, L2: collecting lens, F: filter, MONO: monochromator, CCD: CCD camera, B: burner, BS: beam splitter, PD: photo diode and BD: beam dump

sufficiently low to avoid optical breakdown. An electromechanical shutter installed in front of the burner is used to block the laser beam for taking measurements of the background (see below).

The scattered radiation along the line of the laser beam was collected at right angles by a camera lens (f/2.8, 300 mm) and projected onto the entrance slit of a spectrometer (Acton Research Spectra-Pro, *f*/4, 150 mm, 5nm/mm dispersion) with magnification factor of 0.5. The spectrometer was rotated such that its entrance slit was parallel to the propagation direction of the laser beam. The slit width of the spectrometer was set at 120 μm. At the exit plane of the spectrometer, an intensified CCD camera (PI-MAX, Princeton Instruments, 25 μm pixel size) was mounted, providing 1024 CCD pixels for collecting the spectral distribution and 256 pixels for the spatial distribution of the major species along the laser beam. However, due to the 18 mm diameter of the intensifier, only ~750 pixels were active in the spectral direction. In all experiments, the CCD camera was used in "gate" mode, which enabled detection of light only when a laser pulse arrived at the measuring location. The gated operation was coordinated by using a timing generator (DG-535, Stanford Research) to bracket the signal event in time. The data collection, storage and processing were performed using WinSpec/32 (Princeton Instruments) software. The gated operation was monitored on a 100 MHz oscilloscope (Hewlett Packard 54600B).

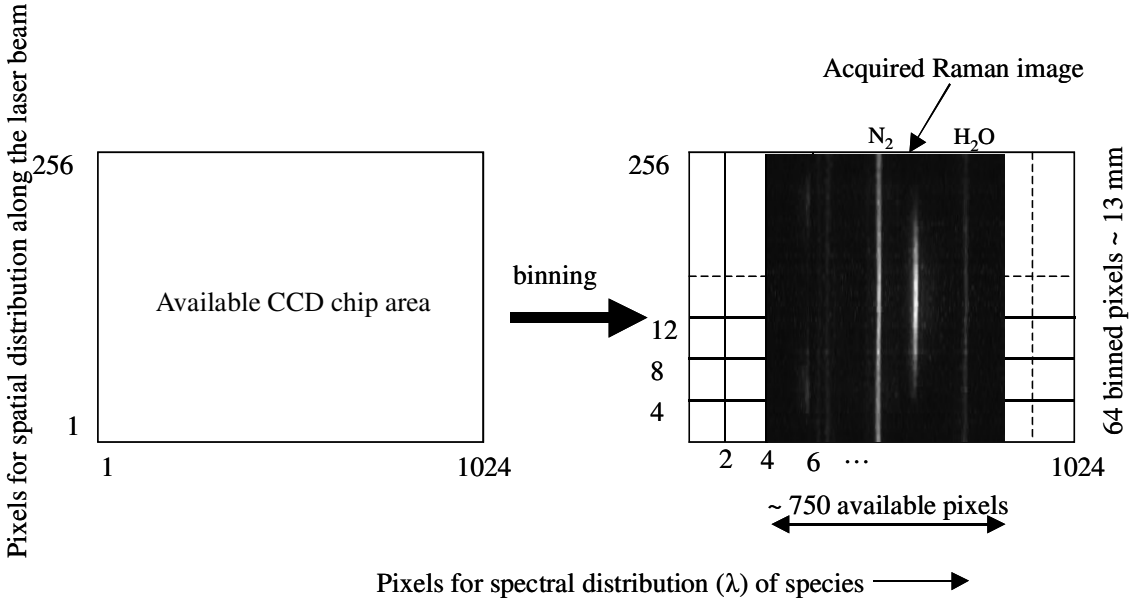

Figure 2.3 CCD binning implemented while collecting the Raman spectra

In coflow diffusion flames, where sharp radial gradients in species distributions are present, it is essential to use every pixel to maximize the spatial resolution.

However, to increase the signal to noise ratio (SNR) while maintaining acceptable spatial and spectral resolutions, the pixels were binned in 2 (in spectral direction) x 4 (in spatial direction) groups in the current work (Fig. 2.3). This resulted in covering a distance ~13 mm (256 pixels x 25 μm pixel size /0.5 magnification) along the laser beam, with the spatial resolution ~ 0.2 mm (25 μm pixel size x 4 binning /0.5 magnification). To measure an entire radial flame profile (~ 25 mm), the Raman spectra were measured around radial positions of 0, +6 and -6 mm and then pasted together, as will be discussed in Ch. 4 and 5. The spectral resolution was approximately 0.5 nm, which was sufficient to resolve the vibrational Raman lines for all major flame species. At every point, 50 accumulations with 10s exposure time were measured with the laser shutter open (Raman signal + background) and closed (background only), and subsequently subtracted. This yielded acceptable SNR even at high flame temperature.

Figures 2.4 –2.6 show the examples of the Raman images acquired in room air and in flames. Figure 2.4 is the example of one of such images in room air, where the

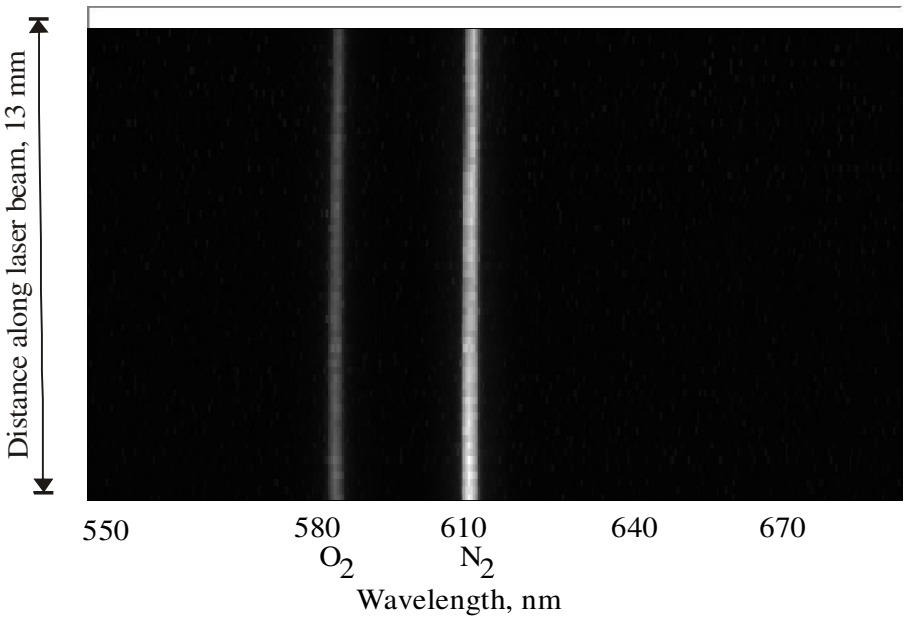

Figure 2.4 Example of a Raman image acquired in room air

Raman bands of N_2 and O_2 can be seen at wavelengths ~ 610 and 580 nm, respectively. As in the room air the spatial distribution of N_2 and O_2 is constant, the Raman bands for these molecules in the image are also uniform along the spatial direction. Figure 2.5 shows the acquired Raman image of the major species at 3 mm height in the region around the axis in a laminar nonpremixed H_2/air flame. In this

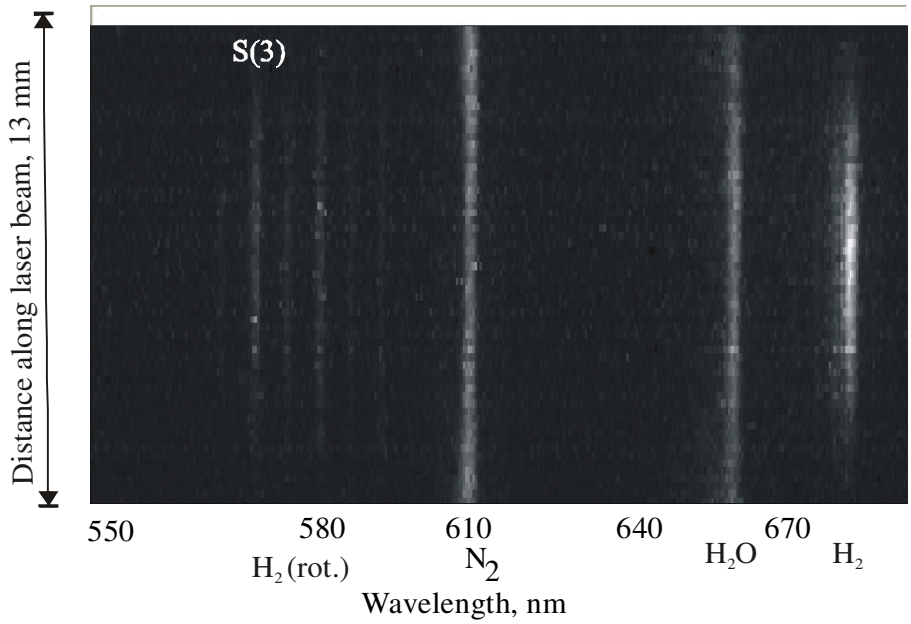

Figure 2.5 Acquired Raman image in the fuel region of a laminar nonpremixed H_2/air diffusion flame

image, the intense H_2 Stokes Q branch in the center is clearly visible at the wavelength region ~ 680 nm. H_2 molecule is also known to produce strong pure rotational Raman lines in the spectral region around 580 nm, which is also evident in Fig. 2.5. Figure 2.6 shows the Raman image acquired in the axial fuel region of a

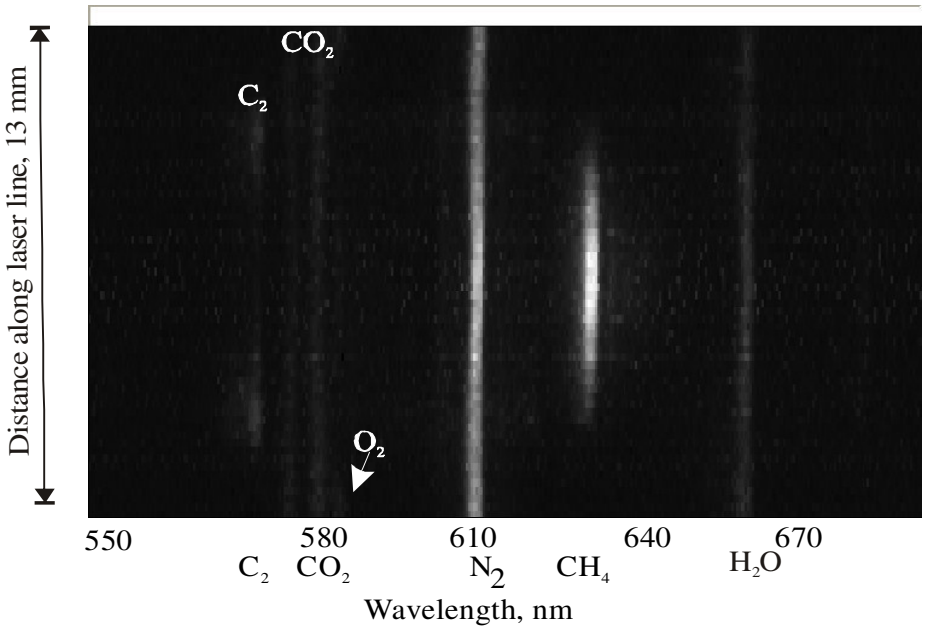

Figure 2.6 Distribution of the major species along the laser beam direction as observed during Raman measurements in the fuel region of a laminar nonpremixed CH_4/air flame

laminar nonpremixed CH_4/air flame. In this image, the fuel CH_4 is clearly observable in the wavelength region ~ 630 nm. We can also observe that the CO_2 Stokes Q branches are present next to the O_2 Stokes branch at ~580 nm wavelength. Interestingly, we see the presence of C_2 fluorescence at the edge of the flame.

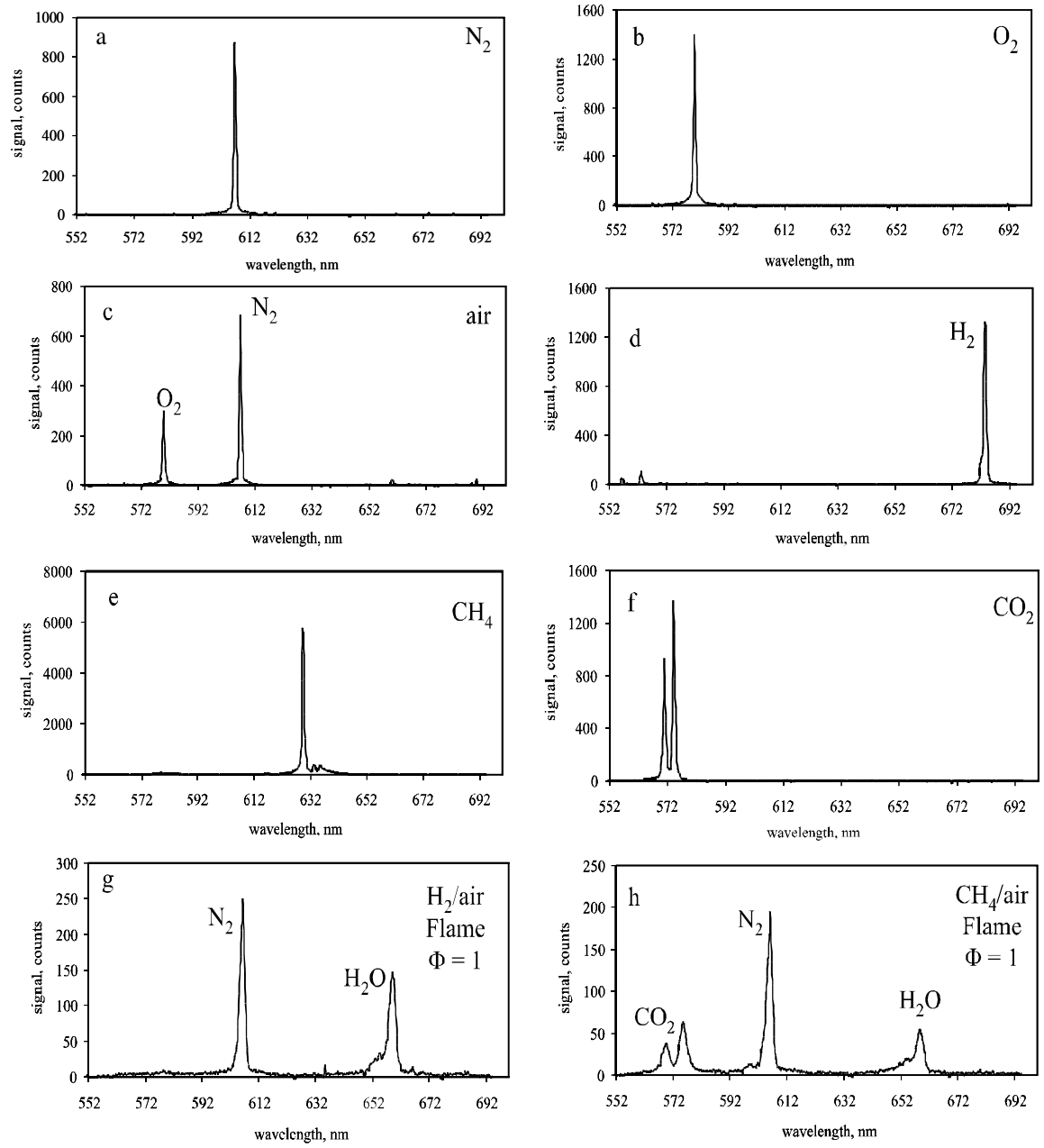

Figure 2.7 Raman spectra collected in air, pure gases and in premixed flames

When the Raman measurements were conducted in media with uniform species distribution, binning all 256 CCD pixels in the spatial direction was possible. This procedure greatly improved the SNR. Figure 2.7 shows the examples of the Raman spectra collected in room air, in individual pure gases at room temperature, and in

premixed flames of H_2/air and CH_4/air. The individual gases: N_2 (Fig. 2.7a), O_2 (Fig. 2.7b), H_2 (Fig. 2.7d), CH_4 (Fig. 2.7e) and CO_2 (Fig. 2.7f) were passed through a premixed flame burner (McKenna Products Inc.) and the Raman spectra of these gases were collected at a location just above the burner exit. The measuring location, being well inside the burner area, ensured uniform species distribution during the measurements. Quantitative aspects of the Raman measurements will be discussed in Ch. 3.

2.3 Coherent anti-Stokes Raman scattering (CARS)

2.3.1 Introduction

Over the past two decades, coherent anti-Stokes Raman scattering (CARS) has evolved into one of the major diagnostic tools for combustion research. This technique has seen many applications to both laboratory and practical combustion systems [10]. Although the technique is relatively complex in its experimental setup and theoretical description, it has survived to become a viable tool due to its unique ability to provide temperature measurements, even in hostile and particle-laden environments [11]. The CARS method had already been demonstrated in mid-1960s [12], but its potential for the study of combustion was realized only in mid-1970s [13]. Although in the present experimental arrangement temperatures can be derived from the Raman measurements themselves (see Ch. 3), we also used CARS to measure temperatures, because of its superior precision.

2.3.2 Background

In CARS, three laser beams at frequencies ν_P and ν_S (usually termed the pump and Stokes beams, respectively) are focused to a common point in the gas sample. Interaction of the laser light with the gas molecules generates light with the frequency ν_{CARS}, which is given as $\nu_{CARS} = 2\ \nu_P - \nu_S$, as shown in Fig. 2.8. Generally, the intensity of the CARS signal is written as

$$I_{CARS} = \left[\frac{4\pi\nu_{CARS}}{c^2}\right]^2 I_P{}^2 I_S \left|\chi^{(3)}{}_{CARS}\right|^2 l^2 \qquad (2.2)$$

where, I_P and I_S are the intensities of the pump and the Stokes beams at ν_P and ν_S, respectively; $\chi^{(3)}{}_{CARS}$ is the third order nonlinear susceptibility and l is the distance.

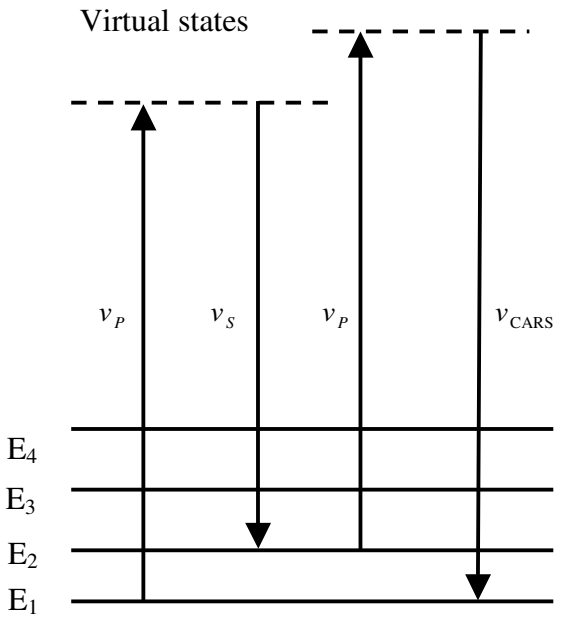

Figure 2.8 Illustration of the CARS process

The non-linear susceptibility indicates the response of the medium with respect to incident radiation.

2.3.3 CARS thermometry

As an example of rotational-vibrational CARS spectrum is shown in Fig. 2.9. The temperature sensitivity of the CARS technique is the result of the variation in

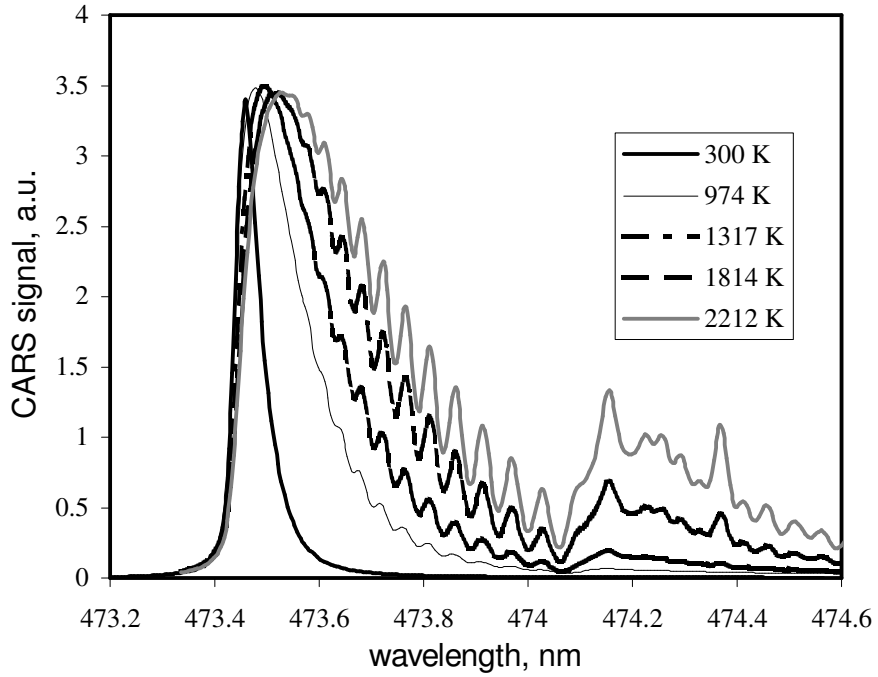

Figure 2.9 Sensitivity of N_2 Q branch CARS spectrum to different temperatures

rotational-vibrational population of the Raman transitions of the species being probed. Thus far, N_2 has received most of the attention as a thermometric species because its abundance in air-breathing combustion. The temperature sensitivity of the N_2 CARS spectrum is illustrated in Fig. 2.9. It can be seen in the figure that at low temperatures the N_2 spectrum is characterized by a strong fundamental band ($v = 0 \rightarrow v = 1$), whose width increases with temperature because the increased population of higher rotational levels. As the temperature approaches 1000 K, the hot-band transition ($v = 1 \rightarrow v = 2$) becomes visible. Thus, the band shape of the N_2 Q-branch spectrum is a good indicator of temperature. The thermometric data reduction schemes employ a least-squares routine for fitting the calculated data and experimental band-shape.

2.3.4 CARS experimental setup

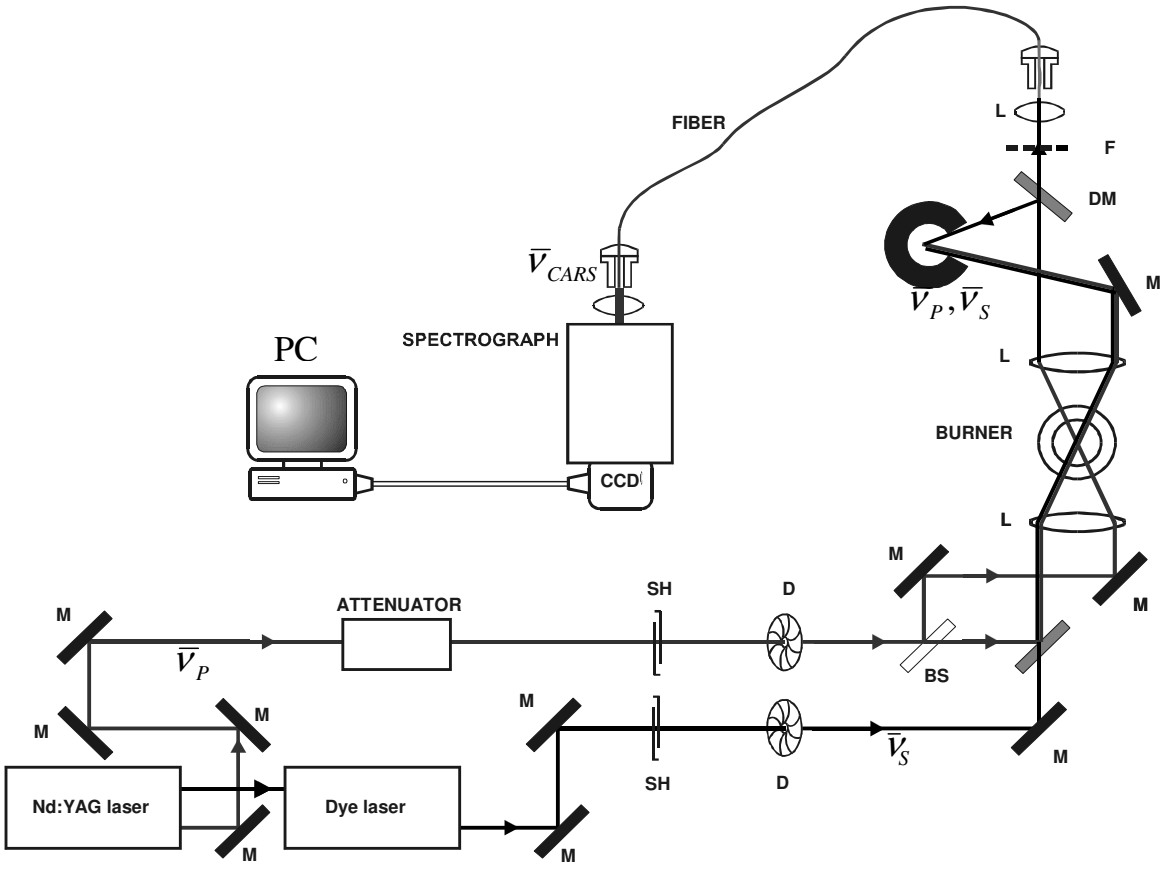

Figure 2.10 Optical setup for the CARS measurements. SH, beam shutter; D, diaphragm; BS, beam splitter; M, mirror; L, lens; BD, beam dumper; PC, personal computer.

Figure 2.10 shows the experimental configurations used for broadband CARS measurements. A Nd:YAG laser (Continuum) at a repetition rate of 10 Hz and with pulse duration of ~ 10 ns generated ~ 500 mJ at a wavelength of 532 nm. 80 % of this

radiation was split off and used to pump a dye laser (Continuum). The dye laser produced up to 60 mJ using the 50-50% dye mixture of Rhodamine 610 and Rhodamine 640. In the oscillator of the dye laser, a grating was replaced by a highly reflecting mirror, producing a broadband output of the order of 100 cm^{-1}. The laser beam at $\bar{\nu}_P$ was directed by a number of mirrors and then was split in two beams by a 50 % splitter. The beams at $\bar{\nu}_P$ and $\bar{\nu}_S$ were arranged in a planar BOXCARS [4] configuration (the distance between beams was ~ 2 cm, and all beam diameters were ~ 1 cm) and were focused with f = 50 cm lens into the measurement area. To position the Stokes beam waist at the crossing point, the adjustable telescope built into the dye laser was used. After spectral separation from the laser beam at ν_P by a dichroic mirror and interference filter, the CARS beam was focused by a short focal length lens to an optical fiber (ϕ ~ 100 μm). At the fiber output, the CARS signal was focused onto the entrance slit of a spectrometer (Jobin Yvon, THR 1000), through one of a series of neutral density filters placed in a filter wheel (ORIEL). The filter wheel was moved by a stepping motor, connected to a computer via an IEEE/488 interface. The broadband CARS signal was detected by an unintensified backlit CCD camera (Princeton Instruments, NTE/CCD-1340/100-EMB) with 1340×100 pixels (25μm). Every measured spectrum was averaged over 100 laser pulses. The spatial resolution of the CARS experiment was determined by the focal volume of diameter ~100 μm and length ~ 1-2 mm.

The CARS spectra were normalized by a nonresonant CARS spectral intensity ("dye spectra") measured in methane. The normalization procedure was necessary to eliminate the dependence of the spectrally resolved CARS spectrum on the spectrum of the dye laser, which is not flat. The measurements of the CARS and dye spectra were conducted within a few minutes from each other to minimize the possible variations of the dye spectra. It was observed that the maximum position of the dye spectrum, especially after the dye had been used for several weeks, could be shifted during 20 minutes operation in such a way to lead to a difference in the determined temperature of ~70 K. The temperatures were extracted from the measured spectra by fitting them to those calculated using the CARP-PC (AEA Technology) program [14].

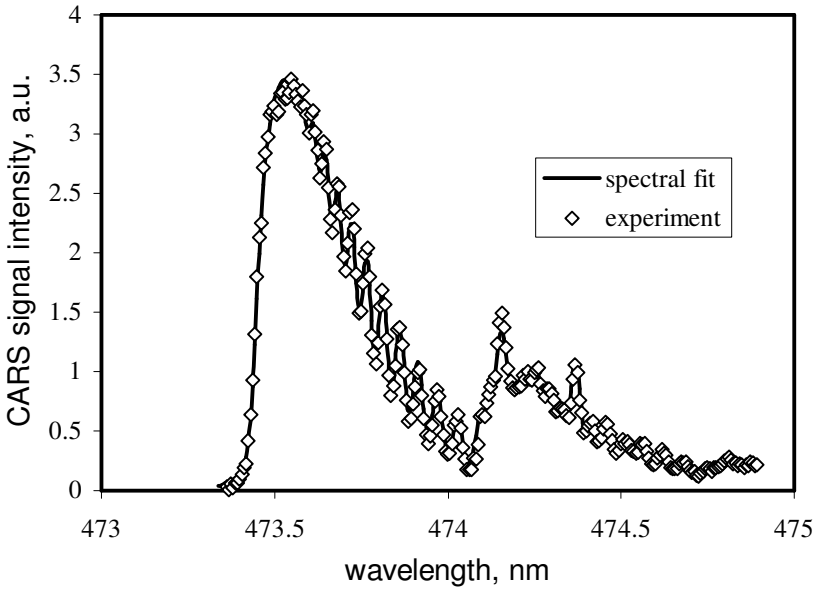

Figure 2.11 Experimental and fitted N_2 CARS spectrum

As an example, Fig. 2.11 shows the measured CARS spectrum of N_2 with a computer fit to a temperature 1900 K. The measurement was made in atmospheric pressure methane-air flame. At this relatively high temperature, the calculated and measured spectra clearly display a two-band structure.

2.4 Laser induced fluorescence (LIF)

2.4.1 Introduction

Raman based approaches, such as spontaneous Raman scattering and CARS, are unable to detect molecular species present in minute amounts due to the inherent weakness of the Raman process. But flame structure studies often demand measurements of intermediate species (which can be present in the parts per million (ppm) level) with sufficient spatial and temporal resolution. As information on these minor species is very important in combustion chemistry, other highly sensitive techniques should be employed. Laser induced fluorescence (LIF) is one such technique, which is capable of measuring concentration of some radical species at the ppm, and even sub-ppm levels [15,16]. In LIF, as shown schematically in Fig. 2.12, the molecule under investigation is excited to an upper electronic level, and the spontaneous emission from the upper level is detected.

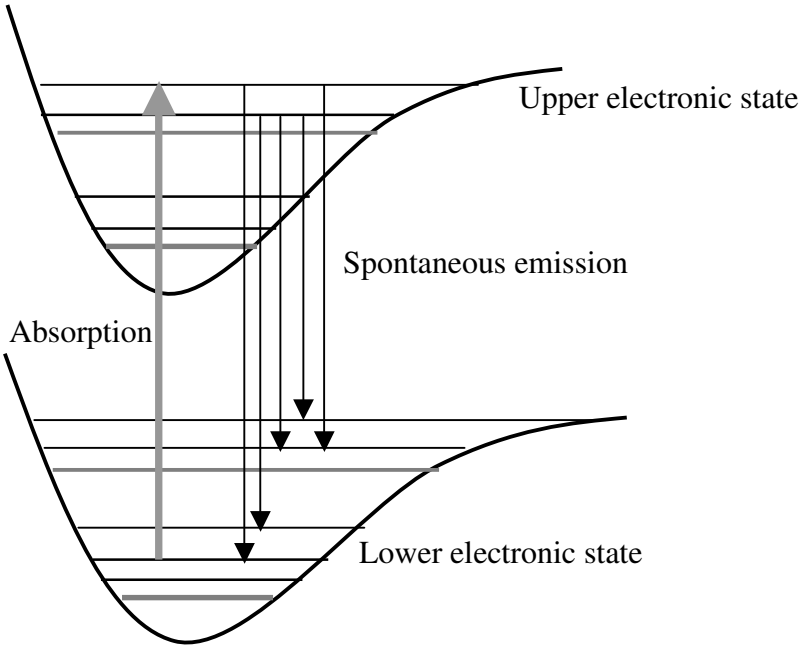

Figure 2.12 Laser induced incandescence (LIF) phenomenon

Often, the detected wavelength is different from the excitation wavelength to avoid the interferences due to Rayleigh or Mie scattering. Resonant absorption has much larger cross section than Raman processes. Therefore, LIF is orders of magnitude stronger than Raman scattering, providing higher detection sensitivity [17]. The fluorescence signal F can be written as,

$$F = h\nu N_2 A_{21} \frac{\Omega}{4\pi} lA\,, \tag{2.3}$$

where $h\nu$ is photon energy, Ω is the collection solid angle, l is the axial distance along the laser beam, A_{21} is the spontaneous emission rate and A is the focal area of the laser beam. At low laser irradiances, the fluorescence signal is in the linear regime, that is, linearly proportional to the input laser irradiance. In this situation, when depopulating the excited level is dominated by non-radiative transfer to the ground state as result of collisions with surrounding molecules (quenching), the fluorescence signal is determined by following equation:

$$F = \frac{h\nu}{c} A_{21} \frac{\Omega}{4\pi} lA \frac{N_1{}^0 B_{12} I^\nu}{(Q_{21} + A_{21})}, \tag{2.4}$$

where I^ν is the incident laser irradiance, B_{12} is the Einstein coefficient for absorption, Q_{21} is the collisional quenching rate and $N_1{}^0$ is total number of molecules. The term

$\frac{A_{21}}{(A_{21}+Q_{21})}$ is called as the fluorescence yield. The quantitative treatment of the LIF data will be discussed in Ch. 3.

2.4.2 Experimental approach for the LIF measurements of OH

The LIF measurements were performed using a Sirah PrecisionScan tunable dye laser pumped by second harmonic of a Nd:YAG laser (Spectra-Physics, Quanta-Ray PRO, 250-10) with 10 ns pulse duration. The laser setup generated radiation at ~310 nm wavelengths with bandwidth ~0.5 cm^{-1} by frequency doubling the dye output. The laser beam was focused onto the test location by a quartz lens (f = 850 mm), as shown in Fig. 2.13. The fluorescence from the flame was collected by a Nikon quartz camera lens (f/4.5, 105 mm) and focused onto the entrance slit of a spectrometer (Acton Research Spectra-Pro 150, f = 150 mm). The entrance slit was set at 120 µm opening

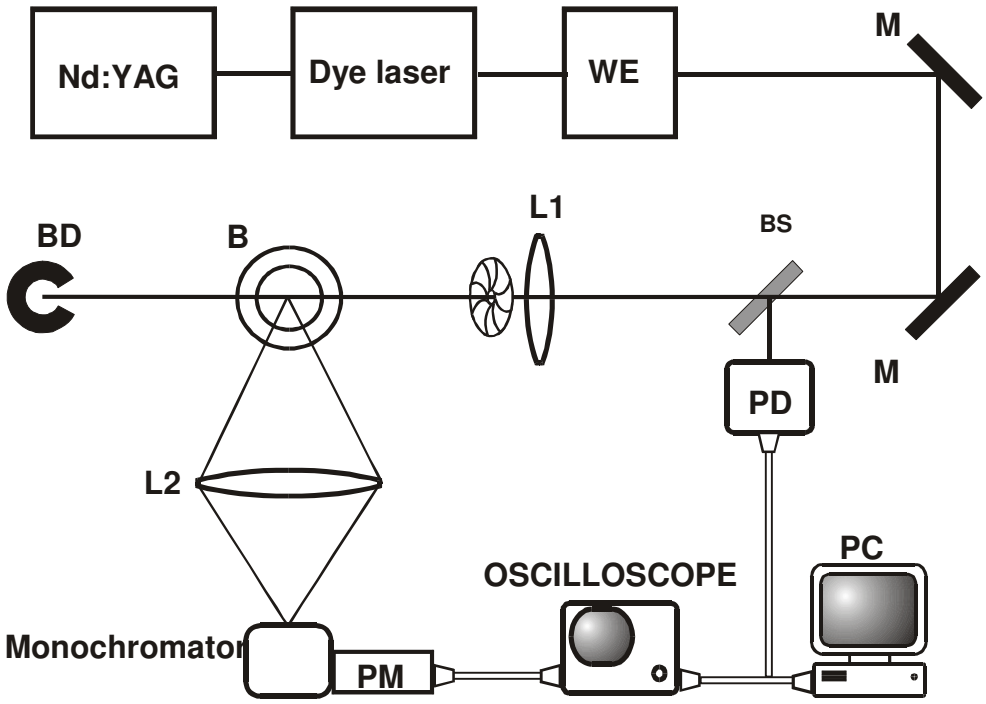

Figure 2.13 LIF optical setup, where WE: wavelength extender, M: mirror, BS: beam splitter, L1: focusing lens, L2: collecting lens, B: burner, PD: photo diode, PMT: photo multiplier tube

and the exit slit was widely open. A photomultiplier (PMT) tube (Electron Tubes 9659QB) was used to measure the fluorescence signal. The entrance slit of the spectrometer was oriented in a direction perpendicular to the laser beam propagation.

The spatial resolution was ~ 0.5 mm. The LIF measurements were performed by exciting the $R_{21}(3.5)$ $A^2\Sigma$-$X^2\Pi$ (0,0) transition of the OH molecule at ~ 308 nm, while the fluorescence was detected at wavelengths centered at 318 nm. The LIF signal was digitized and averaged over 64 laser pulses by a 500 MHz oscilloscope (Hewlett Packard 54615B) with an 8-bit analog-digital converter.

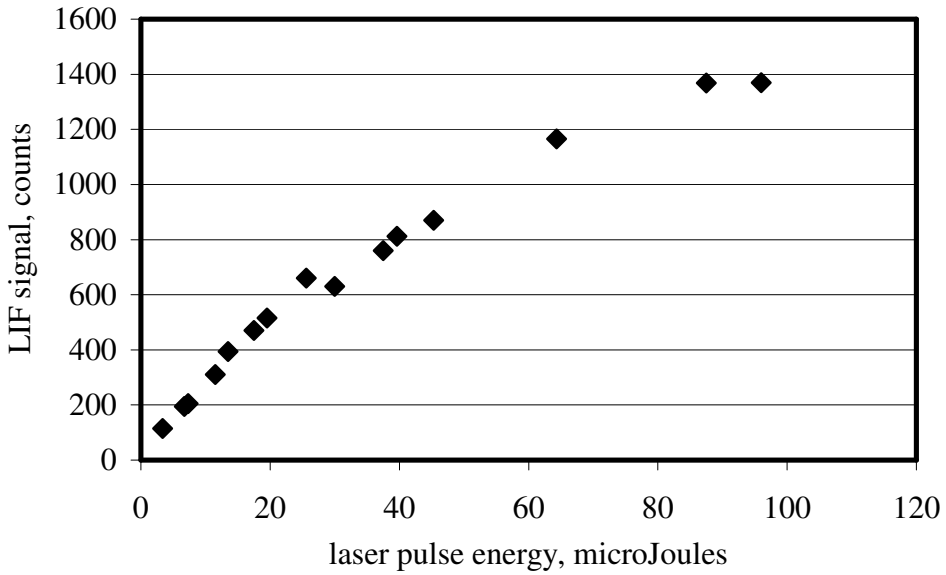

Figure 2.14 Linearity plot showing LIF signal variation over the range of incident laser power

Figure 2.14 shows variation of the LIF signal intensity with incident laser power. As can be seen, the fluorescence signal starts to saturate at high laser energy (≥ 40 μJ). In the experiments, the laser pulse energy was < 20 μJ, low enough to guarantee the linear LIF regime.

2.5 Direct laser absorption

2.5.1 Introduction

Direct laser absorption is a line-of-sight method, in which there is a direct relation between the measured signal and the concentration of the measured species. This technique is often used to calibrate relative profiles of trace species obtained through other techniques, such as LIF. In the present work, this method was used to calibrate the OH LIF profiles obtained in premixed flames, which in turn was used to quantify OH LIF data in the diffusion flames. If broadband light from a source is passed through a medium containing absorbing gas, the intensity of the transmitted light may show a frequency distribution similar to that depicted in Fig. 2.15. If this is

the case, the gas is said to possess an absorption line at the frequency ν_0. In the case of a spatially uniform absorbing medium, the intensity of the transmitted light is obtained from the Beer-Lambert law as,

$$\frac{I}{I_0} = e^{-\alpha l} \tag{2.5}$$

where α is the absorption coefficient and l is the length in the medium over which absorption has taken place.

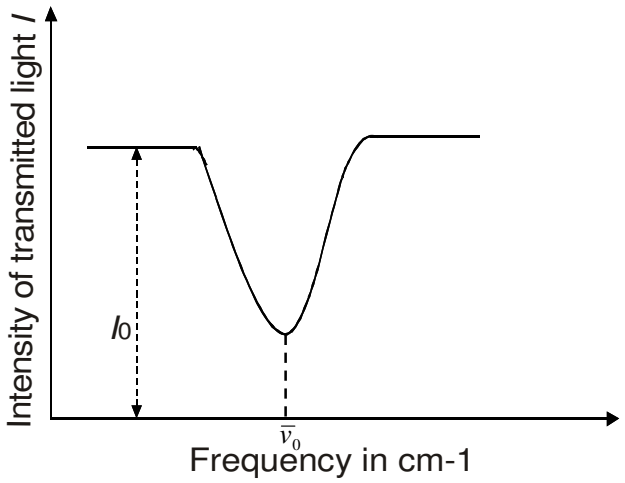

Figure 2.15 An absorption line in broadband excitation.

In real systems, the absorbing medium is spatially non-uniform in many situations. In this case, Eq. 2.5 can be rewritten as,

$$\ln\left(\frac{I_0}{I(\nu)}\right) = \int_0^L \alpha(\nu, l)dl \tag{2.6}$$

where L is the length of the absorbing layer, $I(\nu)$ is the intensity of the transmitted light at ν, I_0 is the intensity of the incident laser beam, α is the absorption coefficient of the medium at frequency ν at the point located at a distance l from the detector.

2.5.2 Experimental setup and procedure

Experimental setup for the direct absorption measurements is shown in Fig. 2.16. As shown in the figure, a laser beam from a Nd:YAG laser (Spectra-Physics,

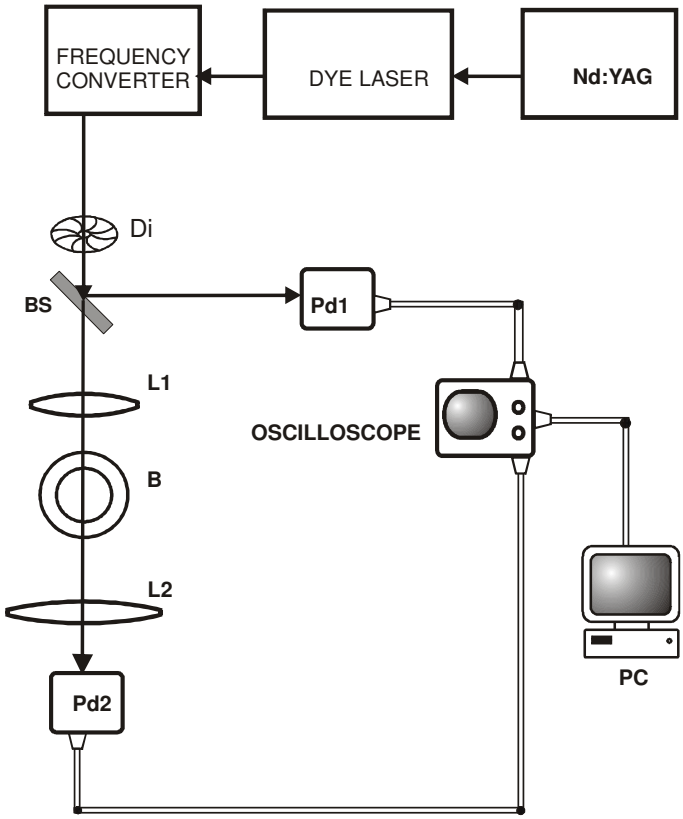

Figure 2.16 Optical setup used for the absorption measurements, where Di: diaphragm, BS: beam splitter, L1: focusing lens, L2: camera lens used to focus on the photodiode Pd2, Pd1: photodiode 1, Pd2: photodiode 2 and B: burner

Quanta-Ray PRO 250-10) pumped a tunable dye laser (Sirah PrecisionScan) with wavelength extender. The laser setup generated radiation at wavelength ~308 nm, with bandwidth 0.5 cm^{-1} and pulse duration 10 ns after frequency doubling the dye output. The laser beam was then focused onto the burner location by a quartz lens (f = 850 mm). Before passing through the focusing lens, a part of the beam was diverted towards a photodiode (Newport, 818-BB-22). The other part of the beam, after passing through the burner location, was focused on the second photodiode (Newport, 818-BB-22) by a lens. The signals from both photodiodes were digitized by a 500-MHz oscilloscope (Hewlett Packard 54615B) and processed by a PC.

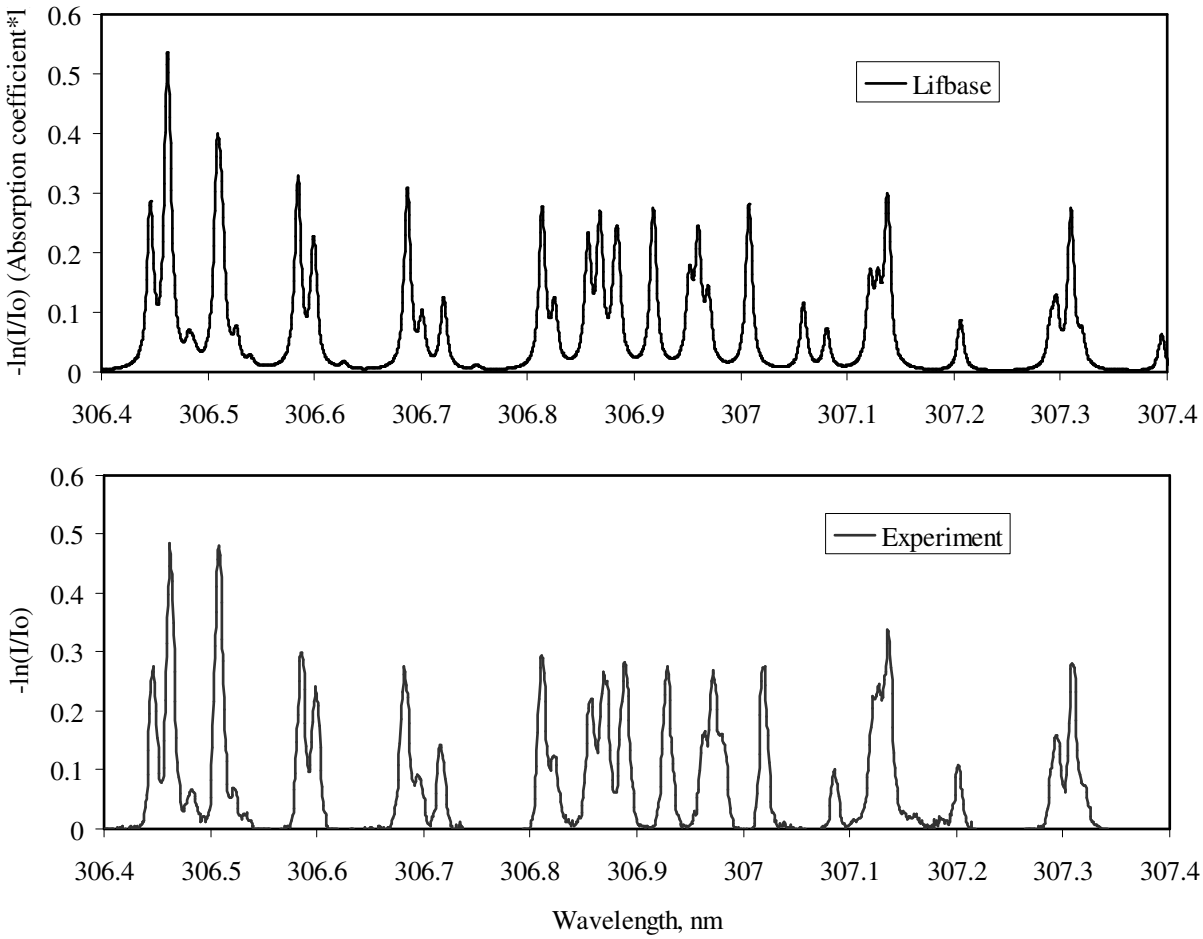

Figure 2.17 Calculated and measured OH excitation spectra

Figure 2.17 shows an example of typical excitation scans performed during direct absorption measurements in a premixed CH_4/air flame (ϕ = 1) at a distance 15 mm above the burner surface. The experimental results are compared with the excitation spectra calculated using the LIFBASE [18] program. We can observe from Fig. 2.17 that there is good agreement between the calculated and measured spectra. The line positions and the spectral features in both plots are coincident.

2.6 Burner setup

2.6.1 Coflow diffusion flame burner and flow arrangement

The coflow diffusion flame burner used in the present study is shown in Fig. 2.18. An upright stainless tube (45.5 cm length, i.d. 0.9 cm) was used to carry the fuel,

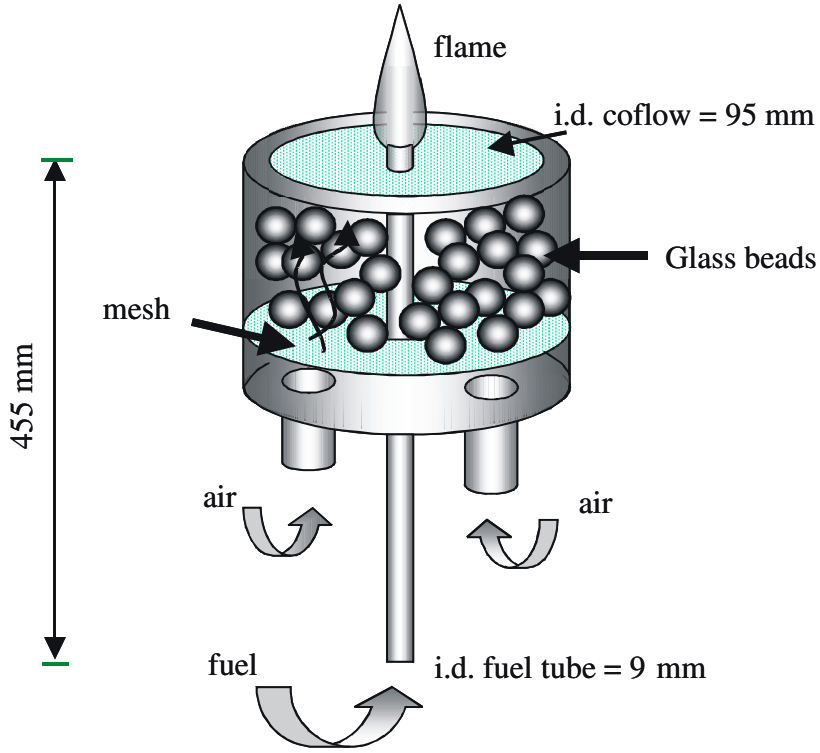

Figure 2.18 Schematic of the diffusion flame burner

surrounded by an air-coflow annulus (i.d. 9.5 cm). The velocity profile in the coflow is homogenized by a settling chamber 10 cm high filled with glass beads, and by using a perforated plate at the exit plane to increase the pressure drop. The fuel tube protrudes 0.8 cm out of the coflow exit plane, so that the small jets generated by the perforated plate can relax to plug flow. The length of the fuel tube (45.5 cm) was sufficient to obtain the fully developed parabolic flow profile, which was verified at the exit of the tube by hot-wire anemometry. In all the experiments, the coflow exit velocities were set equal to the fuel exit velocities.

The flow scheme for the burner feed gases and the coflow air is shown in Fig. 2.19. The flow rates of all the gases were measured using calibrated mass flow meters (Bronkhorst, EL-FLOW) and monitored on a display module (Bronkhorst). All the

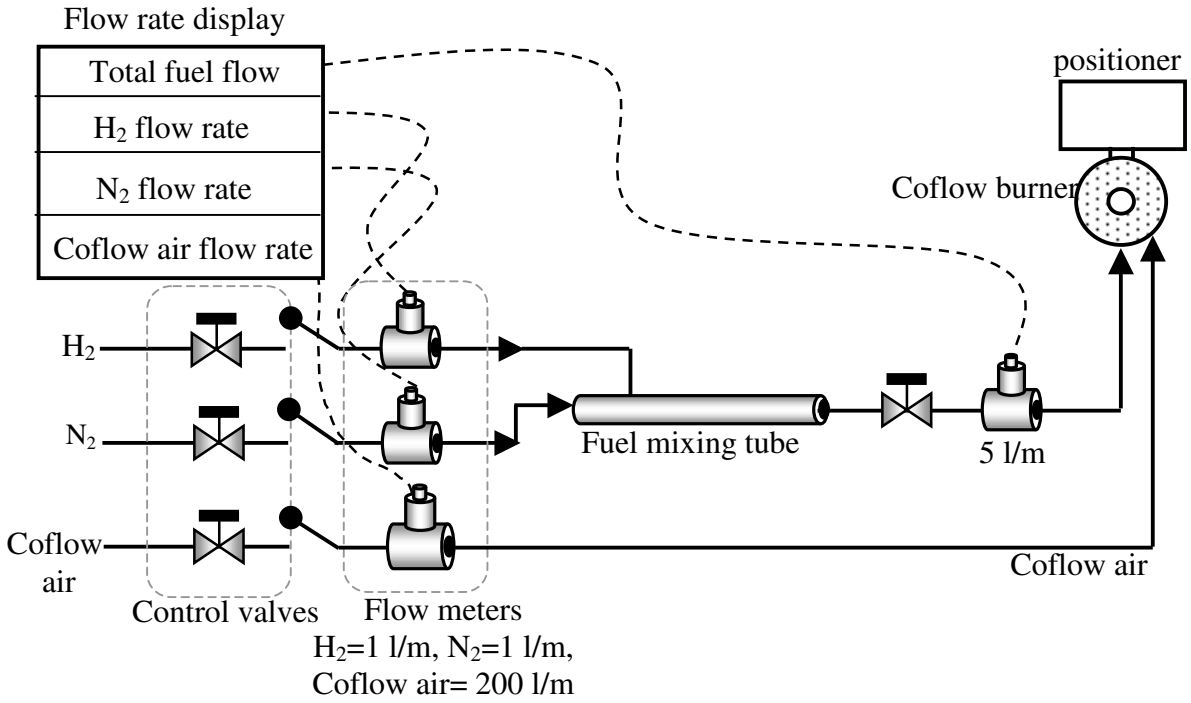

Figure 2.19 Schematic of the flow arrangement for the coflow diffusion flame study

flow meters were initially factory calibrated for N_2 at normal conditions. To obtain the flow rates using these meters for gases other than N_2 at operating conditions, factory conversion factors were used. The flow ranges of the meters were selected to provide

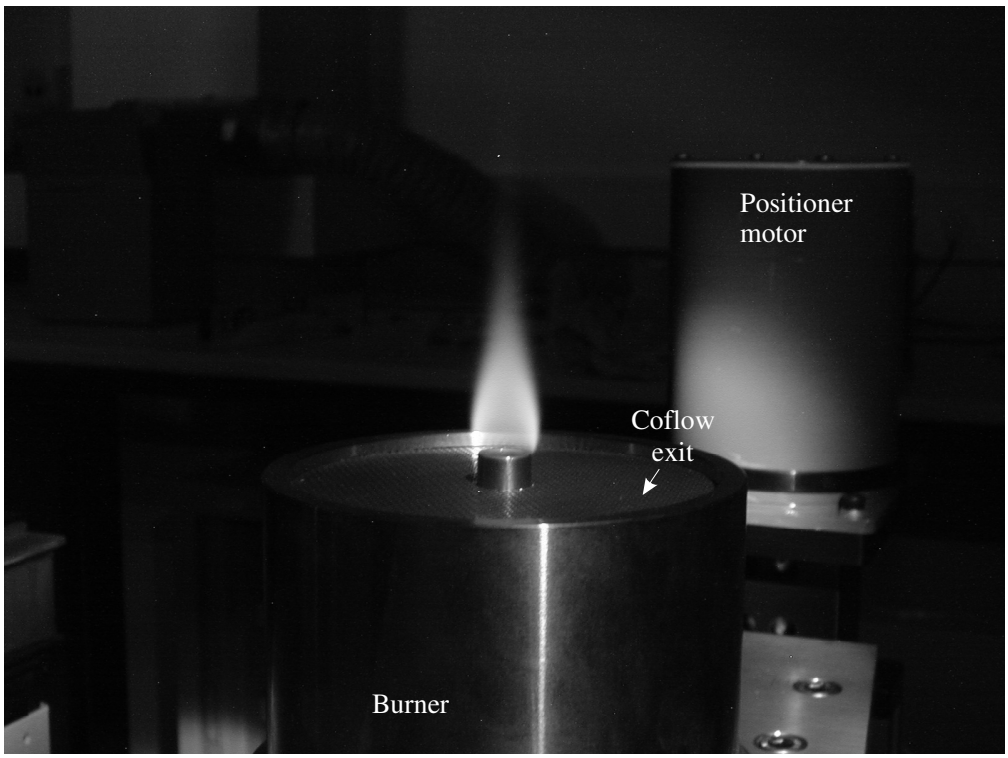

Figure 2.20 Laminar H_2 diffusion flame on a coflow burner

the accuracy better than 5%. A precision positioner (Parker Corp.) was used to move the burner in radial and vertical directions, with accuracy better than 0.1 mm.

Figure 2.20 shows a photo of a nonpremixed H_2/air flame obtained on the coflow burner. The visible flame height in this image is ~ 30 mm. All the flames studied in this work were steady in nature, and thus allowed averaging of data in time.

2.6.2 Premixed flame burner and setup

The premixed flame studies (Ch. 3) were conducted on a water-cooled sinter burner (McKenna Products Inc.), which produces stable and spatially uniform premixed flames of ~ 6 cm diameter. The schematic of the flow scheme used to obtain the premixed flames is shown in Fig. 2.21. As shown in the figure, the fuel and the air were mixed in the mixing tube in desired proportions and supplied to the burner. The flow rates of all the gases were measured by calibrated mass flow meters

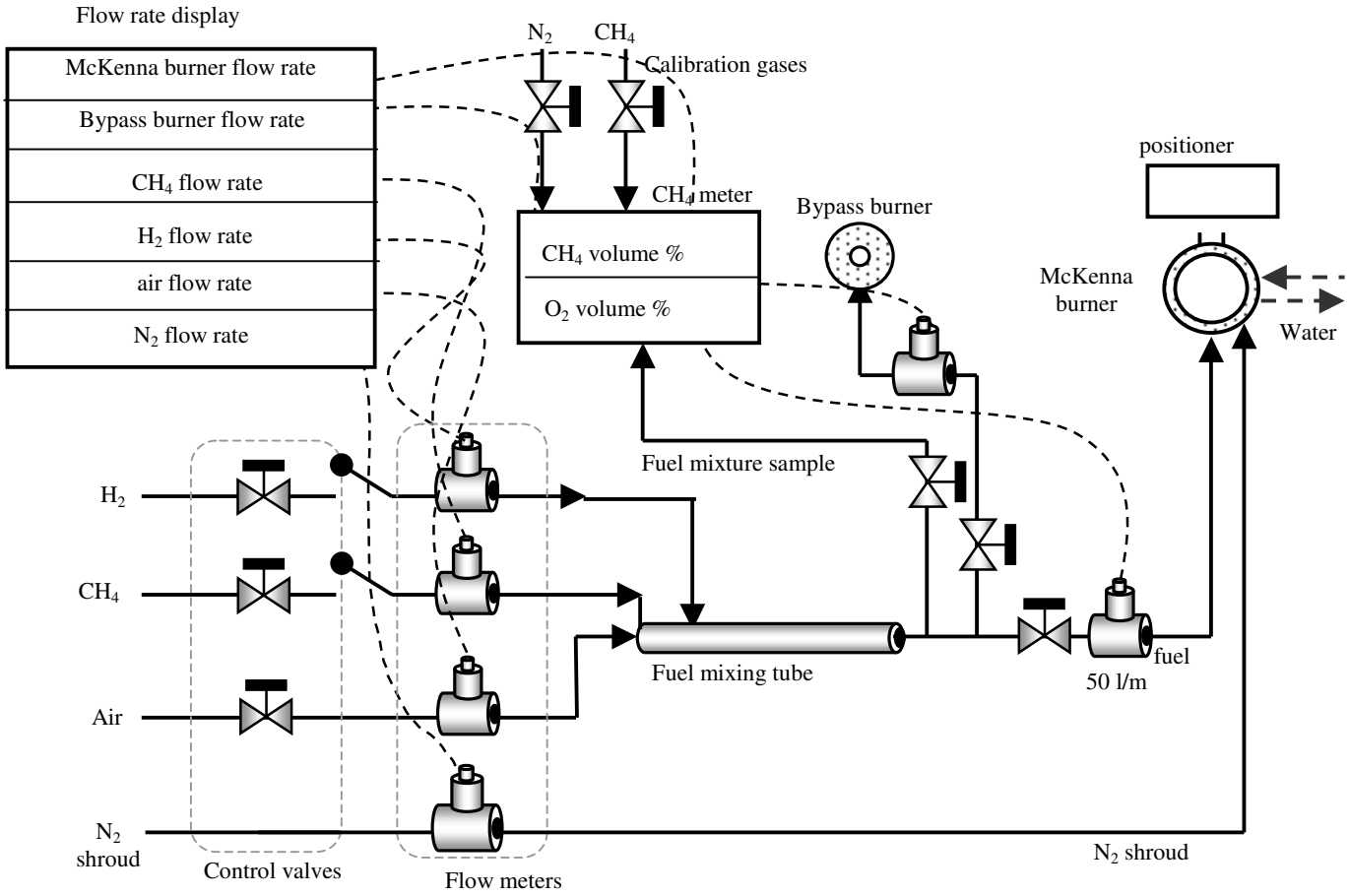

Figure 2.21 Schematic of the flow scheme used for the premixed flame experiments.

(Bronkhorst). The equivalence ratio was determined by measuring the methane or oxygen concentration in the unburned mixture by an infrared and paramagnetic analyzer (Maihak Unor 710). The accuracy of measuring equivalence ratio was better than 2%, with the day-to-day reproducibility better than 1%. In all measurements, a nitrogen shroud was used to prevent mixing of the combustion products with the surrounding air.

2.7 Conclusions

In this chapter, an introduction of the laser techniques used (spontaneous Raman scattering, coherent anti-Stokes Raman scattering (CARS), laser induced fluorescence (LIF) and direct absorption) in this thesis to study the flame structure of laminar H_2/air diffusion flames is provided. The details of the coflow burner and the flow schemes used also have been given.

The Raman scattering data in diffusion flames were measured by collecting the Raman signals of different major species along the laser line. To investigate the structure of coflow diffusion flames, obtaining maximum possible spatial resolution of the species distribution yet maintaining good signal to noise ratio (SNR) in the Raman measurements is important. The binning procedure implemented in this work provided sufficient spatial (0.2 mm) and spectral (0.5 nm) resolutions for the diffusion flame study. With this Raman setup, it was possible to resolve all the spectral features of the flame components. However, the total spatial distance over which the species distribution was collected in every Raman image was insufficient to cover whole radial profile in the diffusion flame. Thus, Raman images at different radial locations should be collected by moving the burner and then pasted together to obtain the whole radial distribution of the major species in diffusion flame. In media with uniform species distribution along the laser line (such as ambient air, premixed flames and cold gases flowing through premixed flame burner), binning of all the CCD pixels in the spatial direction increased the SNR considerably.

The CARS setup provided the spatial resolution for the temperature measurements by ~ 100 μm focal diameter and ~ 1 mm length. The LIF technique was used in the linear regime and the spatial resolution obtained was ~ 0.5 mm. The spectral excitation scans for OH molecule in flames using direct absorption technique revealed excellent qualitative agreement with calculations for similar conditions, providing additional confidence in using this method towards calibrating the LIF OH profiles.

References

1. **M. Lapp, L.M. Goldman and C.M. Penney**, Science 175 (1972) 1112-1115.
2. **M. Lapp and D.L. Hartley**, Combust. Sci. Tech. 13 (1976) 199-210.
3. **S. Lederman**, Prog. Energy Combust. Sci. 3 (1977) 1-34.
4. **A.C. Eckbreth**, "Laser Diagnostics for Combustion Temperature and Species", 2nd edition, Gordon and Breach Publishers (1996).
5. **R.W. Dibble, A.R. Masri and R.W. Bilger,** Combust. Flame 67 (1987) 189-206.
6. **M.D. Smooke, P. Lin, J.K. Lam and M.B. Long,** Proc. Combust. Inst. 23 (1990) 575-582.
7. **M.B. Long, P.S. Levin and D.C. Fourguette,** Opt. Lett. 10 (1985) 267.
8. **J.A. Wehrmeyer, T-S. Cheng and R.W. Pitz**, Appl. Opt. 31 (1992) 1495.
9. **J.A. Shirley,** Appl. Phys. B 51 (1990) 45-48.
10. **W.P. Stricker,** "Applied Combustion Diagnostics" (K. Kohse-Höinghaus and J.B. Jeffries ed.) Taylor and Francis, New York (2002) 155.
11. **W.P. Stricker, R. Lückerath, U. Meier and W. Meier,** J. Raman Spectrosc. 34 (2003) 922-931.
12. **N. Bloembergen, "**Nonlinear Optics", W. A. Benjamin Inc. Publishers, New York (1965) 1-60.
13. **P.R. Regnier and J.P.E. Taran,** Appl. Phys. Lett. 23 (1973) 240-242.
14. **CARP-PC**, a commercially available computer code developed by AEA Technology, Harwell, Didcot, UK, and supplied by Epsilon Research Ltd., High Wycomb, UK.
15. **J.W. Daily**, Prog. Energy Combust. Sci. 23 (1997) 133-199.
16. **K. Kohse-Höinghaus**, Prog. Energy Combust. Sci. 20 (1994) 203-279.
17. **D.R. Crosley,** Opt. Eng. 20 (1981) 511-521.
18. **J. Luque and D.R. Crosley**, LIFBASE: Database and Spectral Simulation Program (version 1.6) SRI International (1999).